Applied Catalysis B: Environmental 134–135 (2013) 349–358

Contents lists available at SciVerse ScienceDirect

Applied Catalysis B: Environmental

journal homepage: www.elsevier.com/locate/apcatb

Tailoring Cu valence and oxygen vacancy in Cu/TiO_2 catalysts for enhanced CO_2 photoreduction efficiency

Lianjun Liu[a], Fei Gao[b], Huilei Zhao[a], Ying Li[a,*]

[a] Mechanical Engineering Department, University of Wisconsin-Milwaukee, 3200 North Cramer Street, Milwaukee, WI 53211, USA
[b] Modern Analysis Center, Nanjing University, 22# Hankou Road, Nanjing, Jiangsu 210093, PR China

ARTICLE INFO

Article history:
Received 8 August 2012
Received in revised form 21 October 2012
Accepted 23 January 2013
Available online 30 January 2013

Keywords:
CO_2 reduction
Photocatalysis
Cu valence
TiO_2
Oxygen vacancy

ABSTRACT

The incorporation of Cu species in TiO_2 photocatalysts is critical in photocatalytic CO_2 reduction to fuels, but the effect of Cu valence is poorly understood. In this work, Cu/TiO_2 (P25) nanoparticle catalysts were prepared by a simple precipitation and calcination method. The as-prepared Cu/TiO_2 sample was dominated by Cu^{2+} species. Thermal pretreatment of the as-prepared samples in He and H_2 atmosphere resulted in the transition to a surface dominated by Cu^+ and mixed Cu^+/Cu^0, respectively, confirmed by in situ X-ray photoelectron spectroscopy (XPS) and diffuse-reflectance infrared Fourier transform spectroscopy (DRIFTS) analyses. These thermal pretreatments in reducing atmospheres also induced the formation of defect sites such as oxygen vacancies and Ti^{3+}. The various Cu/TiO_2 catalysts were tested in CO_2 photoreduction with water vapor under simulated solar irradiation, and their activities were in the order of as-prepared (unpretreated) < He-pretreated < H_2-pretreated. Compared with unpretreated TiO_2 (P25), the H_2-pretreated Cu/TiO_2 demonstrated a 10-fold and 189-fold enhancement in the production of CO and CH_4, respectively. This significant enhancement was mainly attributed to the synergy of the following two factors: (1) the formation of surface defect sites promoting CO_2 adsorption and subsequent charge transfer to the adsorbed CO_2; (2) the existence of Cu^+/Cu^0 couples that facilitate electron and hole trapping at different sites.

1. Introduction

Photocatalytic reduction of CO_2 with H_2O by sunlight is potentially a promising sustainable energy technology that not only reduces the emission of CO_2 but also recycles it back to renewable solar fuels [1,2]. However, the literature reports very low CO_2-to-fuel conversion efficiency by using titanium dioxide (TiO_2), a wide band-gap, cheap, and stable photocatalyst [3,4]. While no active sites are present on a photocatalyst for reactions induced by photoexcited charge carriers (electron–hole pairs) [5], modifications of the photocatalyst will lead to enhanced charge separation and thus improve photocatalytic reaction rate. Various improvement strategies have been developed, including the incorporation of metals (e.g., Rh, Pt, Ag, Cu) [6–10], metal oxides (e.g., CuO_x) [11–16], and nonmetal ions (e.g., N, I) [7,17] on TiO_2, as well as the creation of oxygen vacancies (V_O) in the TiO_2 nanostructure [18,19]. Among these modification strategies, the use of Cu species as a co-catalyst for TiO_2 has attracted much attention, probably due to the low cost and large availability of Cu, and its ability of enhancing CO_2 photoreduction efficiency not inferior to noble metal co-catalysts [7,11].

The role of Cu species in Cu/TiO_2 composites in improving CO_2 photoreduction is not clear in the literature reports. Highly dispersed surface Cu^+ species is reported to be the most active compared to Cu^{2+} and Cu^0 [1,11,12,15,17]. However, Qin et al. [14] demonstrated that it was the heterojunctions between CuO and TiO_2 that contributed to the promotion of the photoactivity, and Slamet et al. [13] suggested that Cu^{2+} was more active than Cu^+ and Cu^0 obtained by H_2 reduction. Only one study in the literature [9] indicated that metallic Cu deposited on TiO_2 will enhance the photoefficiency of CO_2 reduction, where Cu metal played roles both as effective co-catalyst for the reduction of CO_2 and as a reducing species to react with the positive holes simultaneously. On the contrary, Tseng et al. [12] pointed out that the presence of Cu^0 on Cu/TiO_2 decreased the production of methanol product from CO_2. Clearly, it is disputable in the literature what the most active Cu species is as the co-catalyst of TiO_2 for CO_2 photoreduction with H_2O.

In addition, there are uncertainties in the measurement of Cu valence due to its very small concentration on TiO_2, the amorphous nature of dispersed Cu species, and some intrinsic errors involved in material handling and characterization. Heat treatment in reducing atmosphere is usually applied to alter the Cu valence

* Corresponding author. Tel.: +1 414 229 3716; fax: +1 414 229 6958.
E-mail address: liying@uwm.edu (Y. Li).

0926-3373/$ – see front matter © 2013 Elsevier B.V. All rights reserved.
http://dx.doi.org/10.1016/j.apcatb.2013.01.040

from as-prepared Cu/TiO_2 samples. The surface of a H_2-reduced Cu/TiO_2 sample may be re-oxidized when exposed to air before XPS analysis, which was probably caused the XPS to indicate only Cu^+ species rather than expected Cu^0 species, as reported by Li et al. [20]. Similarly, when the H_2-reduced Cu/TiO_2 sample after exposure to air was later tested for CO_2 photoreduction, the Cu valence on the surface may have already changed, thus making it difficult and inaccurate to compare its activity with untreated Cu/TiO_2 sample. Hence, it is very important to use in situ analytical instrumentation and experimental approaches to accurately identify the Cu valence and measure its catalytic activity in CO_2 photoreduction.

Finally, the role of active sites on TiO_2 itself for the Cu/TiO_2 catalyst has usually been neglected in the literature reports on CO_2 photoreduction [11–13]. When preparing Cu/TiO_2 in a reductive atmosphere to form Cu^+ or Cu^0 species, defects such as V_O and Ti^{3+} on TiO_2 were most likely created concurrently due to the oxygen loss [21–24]. However, the effect of these defects or the potential synergies between Cu and the defects were poorly understood. On the other hand, most of the literature publications focused on the application of perfect TiO_2 made by calcination in an air environment; oxygen-deficient TiO_2 for photocatalytic reduction of CO_2 has been rarely reported [19]. Regarding the defect disorders, the theoretical calculations have indicated the benefit of V_O/Ti^{3+} in TiO_2 for promoting the efficiency of H_2O splitting and CO_2 activation [25–27]. Our recent published study for the first time demonstrated the synergy between Cu^+ and V_O/Ti^{3+} for the spontaneous dissociation of CO_2 even in the dark [21]. This work has further advanced the mechanistic understanding in CO_2 photoreduction on Cu/TiO_2 by decoupling the effects of Cu valence from TiO_2 defect sites (i.e., V_O/Ti^{3+}) and exploring the synergies between them under photoillumination. We have fabricated Cu/TiO_2 composites, engineered them with different Cu valences plus V_O/Ti^{3+} sites using a simple method, characterized them by in situ X-ray photoelectron spectroscopy (XPS) and diffuse reflectance infrared Fourier transform spectroscopy (DRIFTS), measured and compared their photocatalytic activities in situ in a special designed photoreactor. New insights in the mechanism of CO_2 photoreduction on Cu/TiO_2 are also discussed in this paper.

2. Experimental

2.1. Catalyst preparation

Cu/TiO_2 was prepared by a simple precipitation method. In brief, 0.5 g of TiO_2 (Degussa P25) was dispersed in 50 ml of 0.25 M NaOH aqueous solution, and then a certain volume of 0.05 M $CuCl_2$ solution (Cu:Ti = 1, 5 at%) was added dropwise under stirring. After further stirring for 6 h, the precipitates were washed with deionized water until pH to 7, and then dried at 80 °C for 12 h. TiO_2 samples without Cu were also prepared in a similar way. Both TiO_2 and Cu/TiO_2 were calcined at 400 °C for 2 h in air.

To prepare Cu/TiO_2 catalysts with different Cu valences, the as-prepared Cu/TiO_2 was in situ pretreated inside the DRIFT reaction cell (for investigation of CO_2 adsorption) or inside the photoreactor (for activity test of CO_2 photoreduction with H_2O) at 220 °C for 1.5 h with a flow of He (99.999%, 120 ml/min) or H_2 (99.998%, 35 ml/min). Bare TiO_2 samples were also pretreated under the same condition. It has been reported that inert gas (e.g., N_2, Ar, He) treatment leads to the formation of oxygen vacancies in TiO_2 and increases the number of electrons in shallow donor states and in the conduction band; each Cu^{2+} ion traps one of these electrons and converts to Cu^+ ion [28]. In a more reductive environment (i.e., H_2), the obtained Cu^+ ions are possibly further reduced into Cu^0 [13]. Hence, our hypothesis was that the as-prepared (unpretreated) Cu/TiO_2 surface would be dominated by Cu^{2+} species, while He and H_2 pretreated Cu/TiO_2 dominated by Cu^+ and Cu^0, respectively. The thermal pretreatment may also result in the formation of V_O/Ti^{3+} sites on TiO_2 and Cu/TiO_2. The unpretreated and pretreated TiO_2 and Cu/TiO_2 samples were denoted as Ti(UP), Ti(He), Ti(H_2), *x*Cu/Ti(UP), *x*Cu/Ti(He) and *x*Cu/Ti(H_2), respectively, where the *x* was the nominal atomic ratio of Cu to Ti, either 1% or 5%, calculated from the Cu and Ti precursor molar concentrations.

2.2. Catalyst characterization

2.2.1. N_2 adsorption–desorption

The surface area, pore size and pore volume of the unpretreated and pretreated 1%Cu/Ti samples were analyzed by nitrogen adsorption at 77 K with the Brunauer–Emmett–Teller (BET) method (Micromeritics, ASAP 2020).

2.2.2. X-ray diffraction (XRD)

The crystal structures of the Cu/TiO_2 samples were identified by X-ray diffraction (XRD, Scintag XDS 2000) using Cu Kα irradiation at 45 kV and a diffracted beam monochromator at 40 mA.

2.2.3. Transmission electron microscopy (TEM)

The lattice structure of Cu/TiO_2 was visualized by phase-contrast high resolution transmission electron microscopy (HRTEM) carried out with 300 keV electrons in a Hitachi H9000NAR instrument with 0.18 nm point and 0.11 nm lattice resolution. Amplitude contrast TEM images were used to obtain the information about the sizes and morphology.

2.2.4. X-ray photoelectron spectroscopy (XPS)

The valence state of Cu was identified by in situ XPS analysis, which was performed on a PHI 5000 Versaprobe system using monochromatic Al KR radiation (1486.6 eV). In the case of pretreated sample, the as-prepared Cu/TiO_2 was placed in the introduction chamber (IC), and then was transferred to the reaction chamber (RC) by a transfer rod. After degassing the RC, the samples were in situ pretreated by introducing He or H_2 into RC at the same conditions as previously described in Section 2.1. As the temperature was cooled down from 220 °C to room temperature, the samples were transferred back to IC, and were degassed again to remove the adsorbed He or H_2. Subsequently, the samples were transferred to the main chamber (MC) for XPS detection. For the unpretreated Cu/TiO_2, the same procedure was performed but without the thermal pretreatment in the RC. All binding energies were referenced to the C 1 s peak at 284.6 eV.

2.2.5. UV–vis diffuse reflectance spectroscopy (UV–vis DRS)

UV–vis diffuse reflectance spectra of the unpretreated and pretreated Cu/TiO_2 were obtained by a UV–visible spectrometer (Ocean Optics) using $BaSO_4$ as the background.

2.2.6. Diffuse reflectance infrared Fourier transforms spectroscopy (DRIFTS)

All IR spectra presented in this work were recorded on a Nicolet 6700 spectrometer (Thermo Electron) equipped with a liquid nitrogen cooled HgCdTe (MCT) detector. The spectra were displayed in absorbance units, and acquired with a resolution of 4 cm^{-1}, using 32 scans. The DRIFTS studies were performed in a Praying Mantis DRIFTS accessory and a reaction chamber (Harrick Scientific, HVC-DRP). The reaction cell is equipped with a heater and a temperature controller, as well as a sample cup in the center. The dome of the DRIFTS cell has two KBr windows allowing IR transmission and a third (quartz) window allowing transmission of irradiation introduced through a liquid light guide (Newport) that connects to a 150 W solar simulator.

The state of Ti on the unpretreated and pretreated Cu/TiO_2 samples was identified by DRIFTS by examining the characteristic Ti–OH bonds. In addition to XPS analysis, in situ DRIFTS experiment was separately performed to confirm the valence of Cu by investigating the adsorption of CO, a probe molecule, on Cu/TiO_2. He-pretreated Cu/TiO_2 samples were in situ prepared by first purging the DRIFTS chamber with He while ramping the temperature to 220 °C at 5 °C/min and then maintaining at 220 °C for 1.5 h in He environment. H_2-reduced Cu/TiO_2 was prepared in a similar manner, and immediately after H_2 treatment at 220 °C for 1.5 h, a relatively high flow rate of He (100 ml/min) was used to purge the DRIFTS chamber to remove surface-adsorbed H_2, if any, until the chamber was cooled down to room temperature. After that, 5%CO balanced in He (Praxair) was introduced into the reaction cell at a rate of 4.0 ml/min at 15 °C. IR spectra were recorded before and after the introduction of CO as the probe molecule.

2.3. In situ DRIFTS for CO_2 photoreduction

The in situ DRIFTS spectra of CO_2 adsorption and activation were recorded on the unpretreated and pretreated $1\%Cu/TiO_2$. In the case of 1%Cu/Ti(UP), the sample was purged by He for 1 h at 25 °C, and the background spectrum in the presence of the sample was collected. After that, $10\%CO_2$ balanced in He (Praxair) passed through the chamber at 2.0 ml/min under photoillumination for 45 min. Meanwhile, the IR spectrum was recorded as a function of time. In the cases of 1%Cu/Ti(He) and $1\%Cu/Ti(H_2)$, the same procedure was used except that the sample was undergone the previously described pretreatment process at 220 °C and the DRIFTS reaction cell was allowed to cool down to 25 °C before the IR spectra were taken.

2.4. Photocatalytic activity measurement

The experiments of CO_2 photoreduction with H_2O on unpretreated and pretreated TiO_2 and Cu/TiO_2 catalysts were carried out in a photoreactor system as described in our previous study [8]. For each test, 50 mg of catalysts was used. For Ti(UP) and Cu/Ti(UP), CO_2 was continuously passed through a water bubbler to bring a mixed gas of $CO_2 + H_2O$ into the photoreactor at a flow rate of 2 ml/min. Ti(He), $Ti(H_2)$, Cu/Ti(He) and $Cu/Ti(H_2)$ were in situ prepared by pretreating Ti(UP) and Cu/Ti(UP) in an He or H_2 environment in the photoreactor using a 250 W infrared lamp to heat up the reactor to 220 °C. After thermal pretreatment, a mixed gas of $CO_2 + H_2O$ at a relatively high flow rate (120 ml/min) was immediately introduced to purge the photoreactor until the reactor was cooled down to room temperature. This step was aimed to remove any surface-adsorbed H_2 from the thermal treatment process. Background measurement by the GC was conducted to verify no H_2 present in the gas phase. After that, the flow rate of $CO_2 + H_2O$ gas was decreased to 2 ml/min for another hour before the photoillumination was turned on to initiate the photocatalytic reaction. A 150 W solar simulator (Oriel) was used as the light source, and the light intensity was about 90 mW/cm^2 in the range of 200–1000 nm. The gaseous products in the reactor effluent were continuously analyzed by a gas chromatograph (GC, Agilent 7890A) equipped with both a thermal conductivity detector (TCD) and flame ionization detector (FID).

3. Results and discussion

3.1. Crystal structure of Cu/TiO_2

The crystal structures of Cu/TiO_2 samples before and after pretreatment were compared by XRD measurement, as shown in Fig. 1. The Cu/Ti(UP) and Cu/Ti(He) samples showed identical mixed

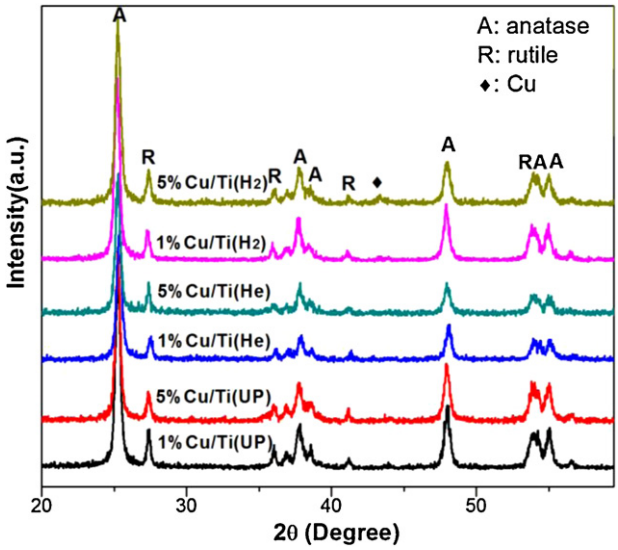

Fig. 1. XRD patterns for unpretreated and pretreated 1%Cu/Ti and 5%Cu/Ti catalysts.

phases of anatase and rutile TiO_2 without appearance of copper oxide or metallic copper, suggesting that Cu species were highly dispersed on the surface. However, a new weak peak for metallic Cu crystal ($2\theta = 43.3°$) [29] were observed on $5\%Cu/Ti(H_2)$, but not on $1\%Cu/Ti(H_2)$. The possible reason for this observation was that at the low loading, the small Cu particles were still highly dispersed even after H_2 reduction; while at the high loading, some Cu species were easily aggregated to larger particles and reduced to metallic Cu^0 by H_2 [12]. It was noted that the diffraction peaks of these He and H_2 treated samples were neither broadened nor narrowed, indicating the crystal phase and size of TiO_2 remained unchanged after the relatively low temperature (220 °C) thermal treatment.

Only the $5\%Cu/Ti(H_2)$ sample was analyzed by TEM and HRTEM because metallic Cu was only observed on this sample and the TiO_2 particle size and morphology were the same as other samples. The TEM image in Fig. 2a showed aggregates of fine nanoparticles with an average size of about 20 nm, agreeing with the primary size of P25 nanoparticles. The HRTEM image in Fig. 2b exhibited clear lattice fringes with an interplanar spacing of 0.350 nm that corresponded to the (1 0 1) plane of anatase [30,31]. The HRTEM image also consisted of the lattice spacing of 0.240 and 0.319 nm that coincided with the (0 0 1) and (1 1 0) plane of rutile TiO_2, respectively [32]. In particular, under the observed projections, other nanoparticles with a size of about 4 nm were seen on the top or the edge of TiO_2. Since the particles were not crystallographically oriented and their sizes were much smaller than that of TiO_2, it may be related to the amorphous Cu species. This HRTEM image directly supported the XRD results that Cu species were highly dispersed on the TiO_2 crystal surface.

3.2. The textual and optical properties of Cu/TiO_2

The textual property of Cu/TiO_2 catalysts was characterized by N_2 adsorption–desorption isotherms. Table 1 compared the results of BET surface area, pore size and pore volume for the unpretreated and pretreated 1%Cu/Ti samples. All three samples had a comparable BET surface area around 50 m^2/g, agreeing with the literature data for TiO_2 P25. The pore size and pore volume for 1%Cu/Ti(He) and $1\%Cu/Ti(H_2)$ were similar, but slight larger than those of 1%Cu/Ti(UP).

UV–vis diffuse reflectance spectra in Fig. 3 showed that the absorption edge of 1%Cu/Ti(UP) is around 410 nm, corresponding to a calculated band gap of 3.04 eV. A slight red shift in the absorption

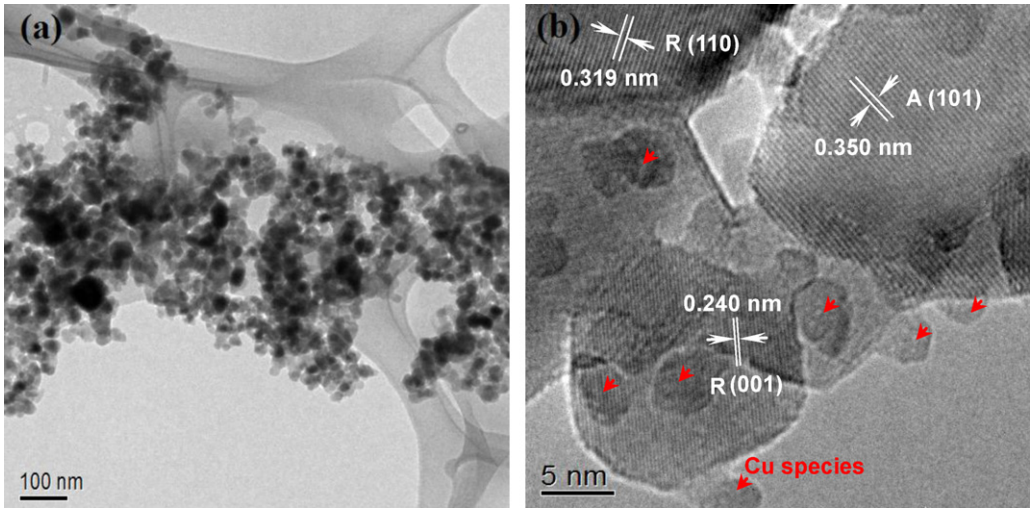

Fig. 2. The TEM (a) and HRTEM (b) images of H_2-reduced 5%Cu/Ti sample. The labeled R and A represented rutile and anatase phase, respectively.

Table 1
The BET surface area, pore size, pore volume, band gap and surface atomic ratio of Cu/Ti for the three 1%Cu/TiO_2 samples.

Samples	BET surface area (m^2/g)	Pore size (nm)	Pore volume (cm^3/g)	Band gap (eV)	Surface atomic ratio of Cu/Ti
1%Cu/Ti(UP)	51.1	19.2	0.246	3.04	0.035
1%Cu/Ti(He)	52.4	24.0	0.315	2.85	0.025
1%Cu/Ti(H_2)	53.7	23.9	0.321	2.89	0.023

edge of 1%Cu/Ti(He) and 1%Cu/Ti(H_2) was observed, resulting in a narrowed band gap at 2.85 and 2.89 eV, respectively. Moreover, 1%Cu/Ti(H_2) had a broad absorption band in the visible range of 430–650 nm, possibly due to the formation of V_O and interstitial H that can harvest visible light and create a color center [22,23,33]. The UV–vis DRS results agree with the physical appearance of the samples reported in Section 3.3.

3.3. The identification of oxygen vacancy and copper valence

A comparison of the DRIFTS spectra of unpretreated and pretreated samples in the range of 3000–3800 cm^{-1} was used to elucidate the existence of Ti^{3+} species. As shown in Fig. 4, for unpretreated sample Cu/Ti(UP) with either 1% or 5% Cu, IR bands at 3693/3635 cm^{-1} were assigned to stretching vibration of OH groups (perturbed by H-bond with H_2O) and that at 3669 cm^{-1} was assigned to Ti^{4+}—OH [32,34,35]. For pretreated samples, Cu/Ti(He) and Cu/Ti(H_2), the original double bands at 3693/3635 cm^{-1} disappeared probably due to H_2O desorption; whereas, a new shoulder at 3717 cm^{-1} appeared, which was assigned to Ti^{3+}—OH [35]. Compared to Cu/Ti(UP), pretreatment also results in not only the increase of the intensity of 3665–3669 cm^{-1} peaks for Ti^{4+}—OH, but also to the appearance of two new weak shoulders at 3615 and 3570 cm^{-1} on Cu/Ti(He) and a new band at 3771 cm^{-1} on Cu/Ti(H_2). Those peaks are possibly related to OH groups experiencing weak intermolecular interactions and the formation of octahedral vacancies, respectively [35,36]. These different IR features suggest that treatment of Cu/Ti facilitates the exposure of more defect sites and OH groups, which probably benefit for CO_2 adsorption and activation. The observations were the same for both 1%Cu/Ti and 5%Cu/Ti samples. This result was in well accordance with the literature that Ti^{3+} and V_O sites were created simultaneously when annealing TiO_2 in an inert or reductive atmosphere [23,24,37,38]. Possible reaction pathways are as follows, where □ represents oxygen vacancy, i.e., V_O.

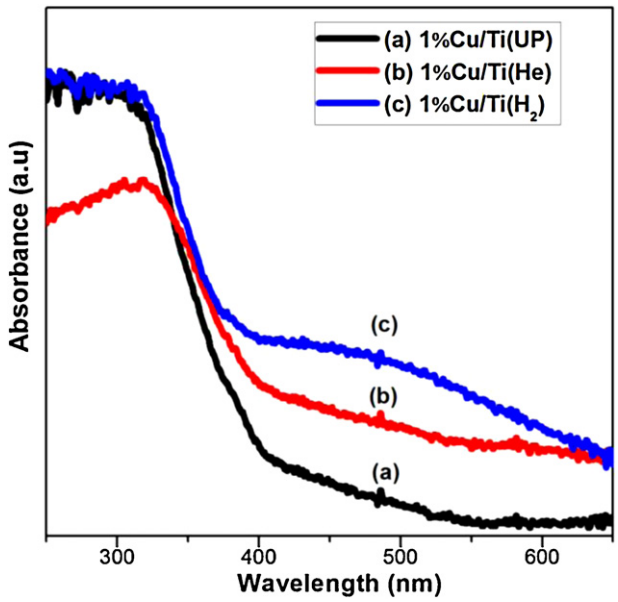

Fig. 3. UV–vis diffuse reflectance spectra of the unpretreated and pretreated 1%Cu/TiO_2.

$$[Ti^{4+}—O^{2-}—Ti^{4+}] \rightarrow [Ti^{3+}—□—Ti^{3+}] + 1/2O_2 \quad (1)$$

$$[Ti^{4+}—O^{2-}—Ti^{4+}] + H_2 \rightarrow [Ti^{3+}—□—Ti^{3+}] + H_2O \quad (2)$$

Hence, the unpretreated Cu/TiO_2 (calcined in an air environment) was relatively defect-free, while He and H_2 pretreated Cu/TiO_2 were defective with V_O/Ti^{3+} sites.

The existence of V_O/Ti^{3+} on the pretreated Cu/TiO_2 was also directly supported by comparing the physical appearance of the catalysts. As shown in Fig. 5, He and H_2 pretreatment induced the change of the initial white color of Ti(UP) to gray and dark gray, respectively. This color transformation was in agreement with the studies by Chen et al. [22] and Danon et al. [23] that the intrinsic defect disorders like V_O and Ti vacancy and hydrogen impurities

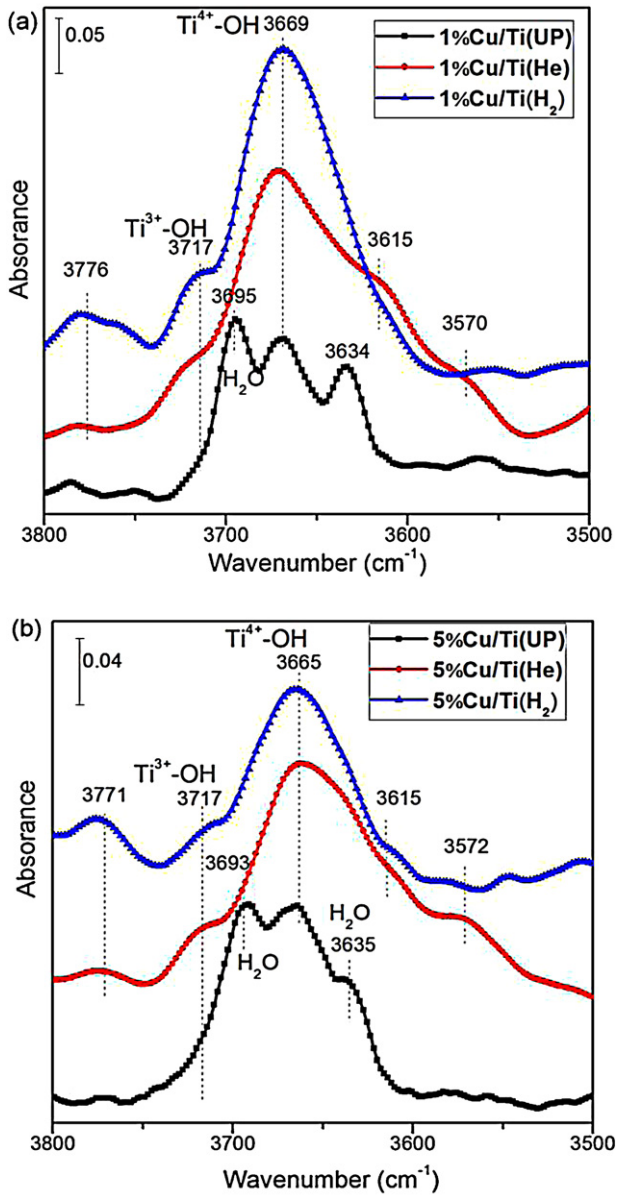

Fig. 4. DRIFTS spectra for the OH group in the region of 3500–3800 cm^{-1} on unpretreated and pretreated Cu/TiO_2 samples.

Fig. 5. Appearance of the various prepared catalysts.

like interstitial H atom on H_2-reduced TiO_2 caused the appearance of black color for their samples. In analogy, 1%Cu/Ti(UP) was light green, while its color turned to brownish and dark cyan, respectively after He and H_2 pretreatment. The colors of 5%Cu/Ti catalysts also in turn changed from gray to dark gray and dark blue. Clearly, the color of pretreated Cu/Ti was significantly darker than that of pretreated TiO_2, possibly because of two reasons: (1) the formation of intrinsic V_O/Ti^{3+} defects and (2) the reduction of Cu^{2+} to Cu^+ or Cu^0. Compared with Cu/Ti(He), the significantly darkened $Cu/Ti(H_2)$ may result from the high content of V_O and the additional interstitial H.

To confirm whether Cu^{2+} was reduced during the pretreatment process, in situ XPS was applied to probe the Cu valence before and after pretreatment. Fig. 6a illustrated the Cu 2p spectra of 1%Cu/Ti samples. For 1%Cu/Ti(UP), two peaks (Cu 2p3/2 at 933.5 eV, Cu 2p1/2 at 953.3 eV) and a satellite peak (at 942.2 eV) for characteristic Cu^{2+} were observed [11,30,39,40]. Two additional peaks for Cu^+ also appeared at 931.4 (Cu 2p3/2) and 951.3 eV (Cu 2p1/2) [12,39,41]. The appearance of Cu^+ was possibly because of the reduction of Cu^{2+} to Cu^+ resulting from the bombardment effect by X-ray irradiation under ultra high vacuum [30], when Cu content was low and existed in a highly dispersed state on the TiO_2 surface. These analyses indicated that Cu^{2+} was the primary species on the 1%Cu/Ti(UP) surface. By contrast, the typical Cu 2p peaks and the satellite peak for Cu^{2+} disappeared on both 1%Cu/Ti(He) and $1\%Cu/Ti(H_2)$. Correspondingly, the signals of Cu^+ increased and were broadened. This change demonstrated that Cu^+ species possibly dominated the 1%Cu/Ti(He) surface. However, the two Cu 2p peaks for Cu^+ could be a mixture of Cu^+/Cu^0 since Cu^+ and Cu^0 have very similar Cu 2p spectra [42]. Due to the difficulty in the identification of Cu^+ and Cu^0 only by binding energy of Cu, the Cu $L_{23}VV$ Auger peaks of Cu were normally applied to distinguish the Cu^+ and Cu^0 from each other [20,30,39]. Unfortunately, no obvious difference was found in the kinetic energies of Cu in our treated samples, possibly due to the very low content of Cu and the charge effect between Cu and TiO_2. Hence, another method, in situ DRIFTS analysis of CO adsorption on Cu sites was applied to explore the change in Cu valence that is described later in this paper.

The same observations for Cu 2p spectrum were also seen on 5%Cu/Ti catalysts, as shown in Fig. 6b. The similar Cu^{2+} and Cu^+ mixture was observed on 5%Cu/Ti(UP). Upon He and H_2 pretreatment, the sharp peaks of Cu 2p3/2 at 931.7 eV and Cu 2p1/2 at 951.5 eV completely replaced the initial Cu 2p peaks and the satellite peak for Cu^{2+}, suggesting that Cu^+ or Cu^+/Cu^0 mixed species were indeed obtained on the treated surfaces. The XPS spectra of binding energies for Ti 2p of 5%Cu/Ti samples are shown in Fig. 6c. Almost identical Ti 2p3/2 (458.0 eV) and Ti 2p1/2 (463.9 eV) peaks were observed on the three 5%Cu/Ti samples, and all the features were assigned to Ti^{4+} [23,30,37,40]. Ti^{3+} species were not detected in the XPS spectra of either 5%Cu/Ti(He) or $5\%Cu/Ti(H_2)$, as opposed to the observation of Ti^{3+} species in the DRIFTS spectra (Fig. 4) and from the color change of the catalysts (Fig. 5). The literature also reported similar findings that surface Ti^{3+} was absent in the XPS spectra of H_2-reduced TiO_2 whereas other characterization methods like electron paramagnetic resonance (EPR) well identified the existence of Ti^{3+} [23,24,37]. It was probably because Ti^{3+} species were in the

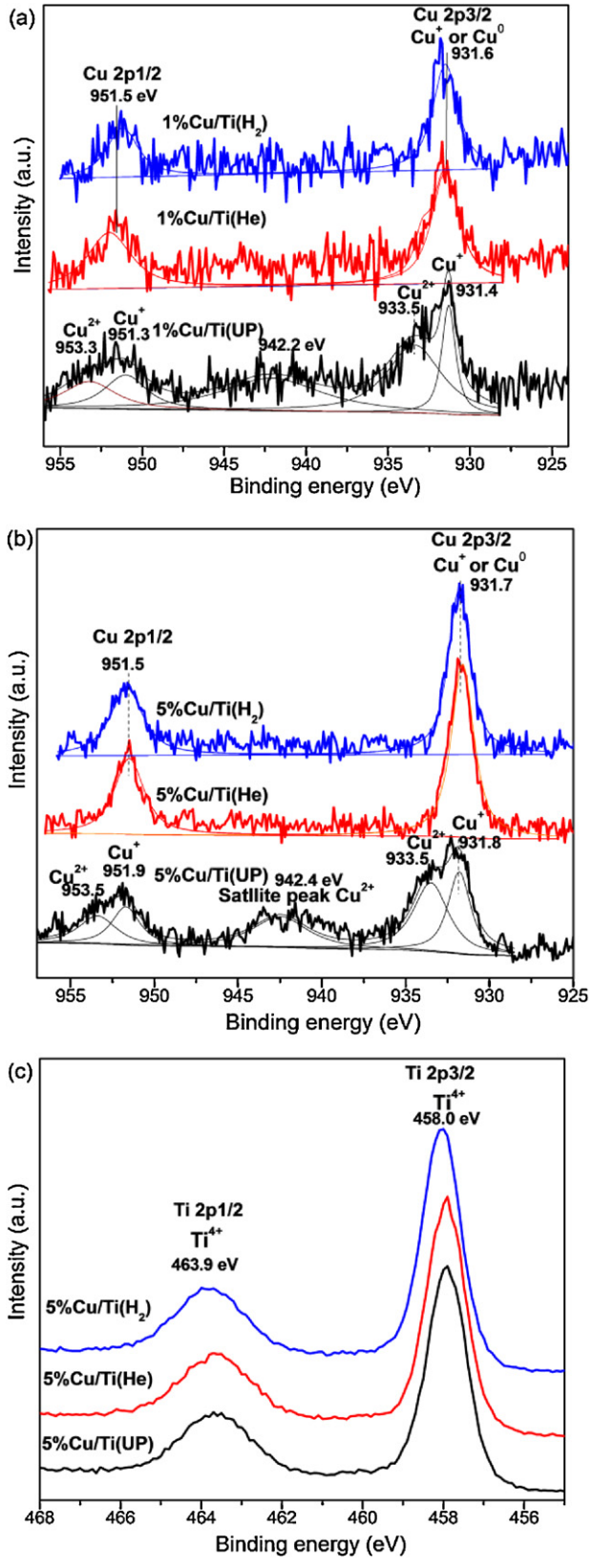

Fig. 6. In situ XPS spectra for (a) Cu 2p of 1%Cu/Ti samples, (b) Cu 2p of 5%Cu/Ti samples, and (c) Ti 2p of 5%Cu/Ti samples.

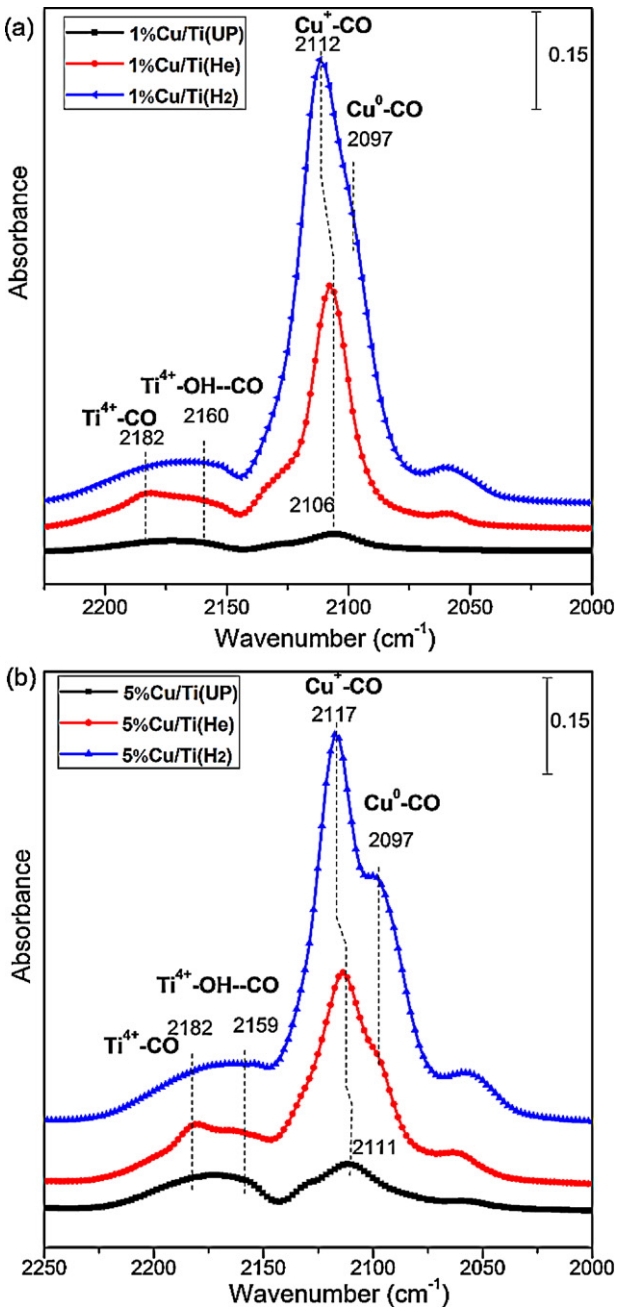

Fig. 7. In situ DRIFTS spectra of CO adsorption on unpretreated and pretreated Cu/Ti samples (a) 1%Cu/Ti; (b) 5%Cu/Ti.

subsurface or the bulk while XPS technique only characterized the top 1–10 nm surface-layer of the materials [37].

XPS was also employed to quantify the real surface Cu concentration compared to the nominal value calculated from precursor concentrations. The data is shown in Table 1. For all the unpretreated and pretreated 1%Cu/TiO_2 samples, the surface atomic ratio of Cu/Ti is in the range of 2–3%, higher than the nominal value (1%), indicating surface Cu concentration is higher than in the bulk.

Because XPS cannot well distinguish Cu^+ from Cu^0 as previously discussed, in situ DRIFTS of CO adsorption was performed to facilitate the identification of the various Cu valences, since CO can be selectively coordinated with Cu^{2+} (2190–2200 cm^{-1}), Cu^+ (2100–2150 cm^{-1}), and Cu^0 (2050–2100 cm^{-1}) at different positions [43–45]. Fig. 7 displayed the IR spectra of CO interaction with various Cu/Ti catalysts. For 1%Cu/Ti(UP) (Fig. 7a), three very

weak bands appeared at 2106, 2160 and 2182 cm^{-1}, which were attributed to the coordination of CO with Cu^+, Ti^{4+}—OH and Ti^{4+}, respectively [46,47]. The Cu^{2+}—CO band expected at 2192 cm^{-1} was not observed possibly due to the weak interaction of CO with Cu^{2+} [43]. By contrast, the intensity of Cu^+—CO band on 1%Cu/Ti(He) was much stronger than that on 1%Cu/Ti(UP), and further increased on 1%Cu/Ti(H_2). In addition, a new shoulder appeared at 2097 cm^{-1} on 1%Cu/Ti(H_2) which could be assigned to Cu^0—CO band [45]. Similar IR spectra for Cu^+—CO and Cu^0—CO were also observed upon CO interaction with 5%Cu/Ti catalysts, as shown in Fig. 7b. Compared to the 1%Cu/Ti(H_2) catalyst, the 5%Cu/Ti(H_2) catalyst showed stronger features of Cu^0—CO, most likely due to the higher Cu concentration. The 5%Cu/Ti(He) catalyst showed a hump-like Cu^0—CO feature, which was not apparent on the 1%Cu/Ti(He) catalyst with lower Cu concentration. The above evolutions of IR spectra clearly indicated that thermal-treatment in He or H_2 reduced Cu^{2+} to Cu^+ and further to Cu^0, forming a mixed Cu^+/Cu^0 state, with a larger fraction of Cu^0 by H_2 treatment. Combining the results from both in situ XPS and DRIFTS analyses, it is reasonable to conclude the following Cu valence states on the prepared Cu/TiO_2 samples: Cu/Ti(UP) has mixed Cu^{2+}/Cu^+ states dominated by Cu^{2+}, Cu/Ti(He) has mixed Cu^+/Cu^0 states dominated by Cu^+, and Cu/Ti(H_2) has mixed Cu^+/Cu^0 states with a higher fraction of Cu^0 than in Cu/Ti(He).

Attempts have been made to prepare single valence Cu^0 on TiO_2 by increasing the H_2 reduction temperature from 220 to 400 °C. However, the in situ DRIFTS spectra of CO adsorption still showed a strong peak of Cu^+—CO and a shoulder of Cu^0—CO, very similar to the spectra shown in Fig. 7 for the Cu/Ti(H_2) sample. This suggests that it is difficult to completely reduce Cu^+ species to Cu^0 possibly because the Cu^+ species are in highly dispersed state. In addition, this is an original work that aimed to qualitatively identify the different Cu valences and TiO_2 defect sites as well as their effects on photocatalytic activity in CO_2 reduction. Quantitative measurements of the Cu valence composition (e.g., the fraction of Cu^+ in the Cu^+/Cu^0 mixture) and surface density of the active sites will be fully investigated in follow-up studies.

3.4. Catalytic activity for CO_2 photoreduction

The photocatalytic activities of the unpretreated and pretreated TiO_2 and Cu/TiO_2 catalysts were measured in the experiments of CO_2 photoreduction by H_2O vapor. CO and CH_4 were found to be the major CO_2 reduction products and no other products were detected, consistent with the findings in our previous studies [15,17] and some literature reports [3,4,16]. Since the reactor was operating in a continuous-flow mode, the production rates of CO and CH_4, in μmol g^{-1} h^{-1}, were recorded as a function of illumination time for all samples (see Fig. 8 for example curves of the CO and CH_4 production rates using 1%Cu/Ti samples). For all the samples tested in this work, including bare TiO_2, 1%Cu/Ti and 5%Cu/Ti, the rates of CO and CH_4 production did not remain steady after reaching their maximum values, but gradually decreased. This decrease in production rate suggests a gradual deactivation of the catalyst, a phenomenon that has been generally observed in CO_2 photoreduction studies, including our previous work [15,21] and other literature reports [48,49]. The exact mechanism of deactivation is not clear, but possible reasons are saturation of the adsorption sites on the TiO_2 surface with intermediate products and/or photooxidation of products back into CO_2 by O_2 produced in the reaction [15,48,50,51].

In this work, the change of catalyst properties may also result in the deactivation. The 1%Cu/Ti(He) catalyst after CO_2 photoreduction reaction was characterized by in situ DRIFTS of CO adsorption; the result indicated that the intensity of Cu^+—CO band drastically decreased after the reaction, compared with the fresh 1%Cu/Ti(He)

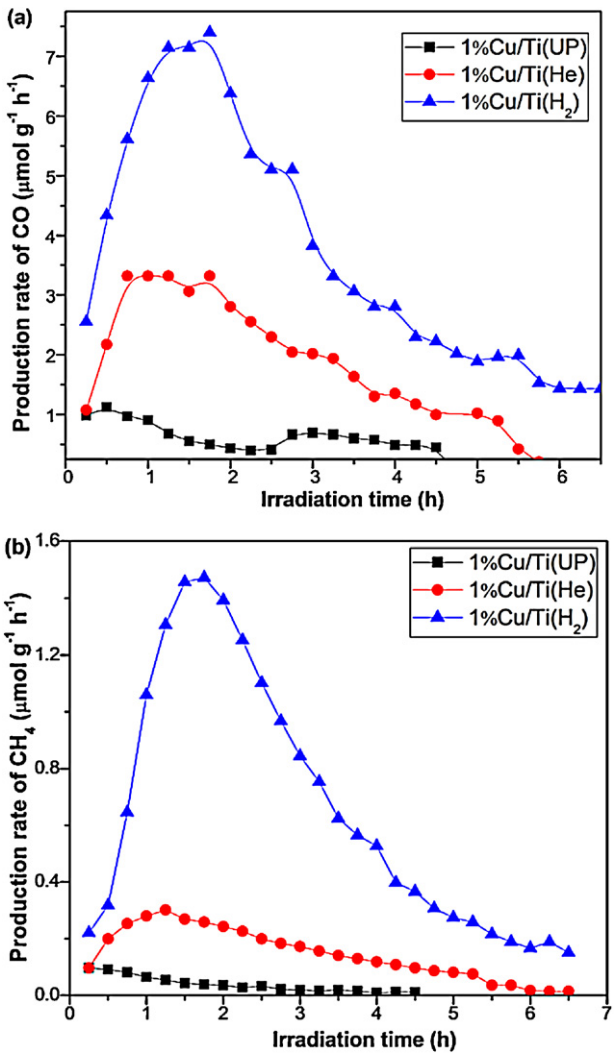

Fig. 8. The production rate of (a) CO and (b) CH_4 on the unpretreated and pretreated 1%Cu/Ti catalysts as a function of photoirradiation time.

sample. This indicates a possible transition of Cu^+ to Cu^{2+} during the photoreaction, with Cu^+ acting as a hole scavenger [21]. In addition, a general observation was that the color of pretreated Cu/TiO_2 catalysts became lighter after CO_2 photoreduction. This may be due to the partial consumption of surface defect sites (i.e., V_O/Ti^{3+}) because the O fragment from CO_2 tends to heal the V_O [27]. The decreasing number of defect sites may also result in reduced CO_2 activation and photoreduction rate. A separate study in enhancing the stability of catalytic performance in CO_2 photoreduction is underway.

Because of the general trend of catalyst deactivating, to better compare the photocatalytic activities of the various samples, the accumulative productions of CO and CH_4 for the period of 6.5 h, in μmol g^{-1}, were calculated by integrating the production rate with illumination time, and the results are summarized in Fig. 9. As shown in Fig. 9a, for bare TiO_2, the production of CO was close to each other on Ti(UP) and Ti(He), but was enhanced by nearly 4 times on Ti(H_2). The incorporation of Cu^{2+} on unpretreated TiO_2 enhanced CO production at a lower Cu concentration (i.e., 1%Cu/Ti(UP)) but reduced CO production at a higher Cu concentration (i.e., 5%Cu/Ti(UP)). Compared to unpretreated Cu/Ti, the ones pretreated by He or by H_2, exhibited remarkable enhancement in CO production, and the order of activity was in the order of unpretreated < He-pretreated < H_2-pretreated. Fig. 9b showed the production of CH_4, which was always lower than that of CO,

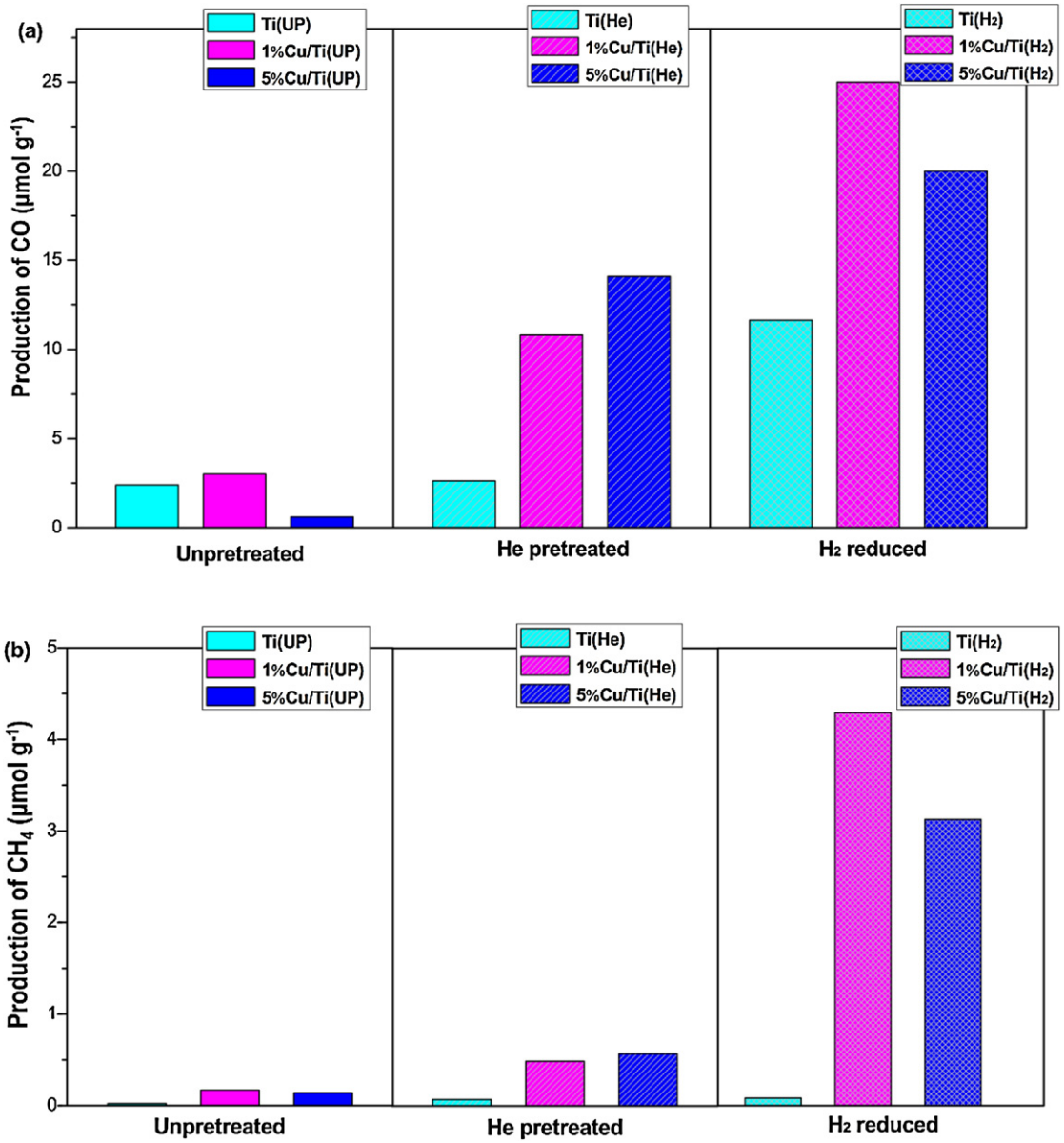

Fig. 9. The production of (a) CO and (b) CH_4 on the unpretreated and pretreated TiO_2 and Cu/TiO_2 catalysts under photoirradiation for 6.5 h.

probably because the formation of one CH_4 molecule requires eight electrons while that of CO requires only two [2,16]. The production of CH_4 on bare TiO_2, pretreated or not, were negligible. The trends in CH_4 production enhancement due to the modification of Cu and He/H_2 pretreatment were similar to those observed in CO production. Among all the catalysts, $1\%Cu/Ti(H_2)$ had the highest activity at 25 and 4.4 $\mu mol\,g^{-1}$ for CO and CH_4 production respectively, demonstrating the superb ability of H_2-treated Cu/TiO_2 for CO_2 photoreduction.

To decouple the potential contributions of Cu species from those of defect sites and to explore the synergy between them, the enhancement factor (F) was calculated, defined by the normalized CO or CH_4 production of a treated TiO_2 or $1\%Cu/TiO_2$ catalyst compared to that of unpretreated TiO_2, as shown in Table 2. The enhancement attributed to the addition of Cu species, to the defect sites formed by pretreatment in He or in H_2, and to the combination of the above two effects are represented by F_{Cu}, F_D and $F_{Cu/D}$, respectively. F_{Cu} is 1.3 and 7.4 for CO and CH_4 production, respectively, indicating the addition of Cu (i.e., Cu^{2+}) enhanced both CO and CH_4 production, because Cu species can inhibit charge recombination by trapping electrons [13,48]. The F_D values are all greater than 1, suggesting the pretreatment of TiO_2 improved CO_2 photoreduction mainly due to the formation of surface defects like V_O/Ti^{3+} sites. The reason of defect sites in facilitating the activation and reduction of CO_2 is described later in this paper using in situ DRIFTS analysis. The F_D for CO production is higher on $Ti(H_2)$ than that on Ti(He), possibly due to the increasing number of V_O/Ti^{3+} sites in a more

Table 2
The enhancement factor (F) of CO and CH_4 production for the treated TiO_2 and 1%Cu/Ti photocatalysts in comparison to unpretreated TiO_2.

Fuels	Ti(UP)	F_{Cu} [a]	F_D [b]		$F_{Cu/D}$ [c]	
		Cu/Ti(UP)	Ti(He)	$Ti(H_2)$	Cu/Ti(He)	$Cu/Ti(H_2)$
CO	1	1.3	1.1	4.8	4.5	10.4
CH_4	1	7.4	3.2	3.5	21.8	188.9

[a] $F_{Cu} = Y_{Cu/Ti(UP)}/Y_{Ti(UP)}$.
[b] $F_D = Y_{Ti(He)}/Y_{Ti(UP)}$ or $Y_{Ti(H_2)}/Y_{Ti(UP)}$.
[c] $F_{Cu/D} = Y_{Cu/Ti(He)}/Y_{Ti(UP)}$ or $Y_{Cu/Ti(H_2)}/Y_{Ti(UP)}$, where Y represents the production of CO or CH_4 as shown in Fig. 8.

reductive atmosphere (i.e., H_2); however, the F_D for CH_4 production is comparable on the two samples, indicating the V_O/Ti^{3+} sites have more significant effect on CO production than on CH_4.

The most important results in Table 2 are the values of $F_{Cu/D}$, which are greater than the sum of their corresponding F_{Cu} and F_D values, clearly demonstrating the synergy between Cu species and surface defect sites. For 1%Cu/Ti(He), the material characterization results showed a dominated Cu^+ species on the surface. These Cu^+ species on Cu/Ti(He) surface can more effectively trap electrons than Cu^{2+} species (as on Cu/Ti(UP) surface) do, because the reduction potential of Cu^+/Cu^0 (0.52 eV) is more positive than that of Cu^{2+}/Cu^0 (0.34 eV) [13]. For 1%Cu/Ti(H_2), the $F_{Cu/D}$ values for CO and CH_4 production are 10.4 and 188.9, respectively, much higher than those on the 1%Cu/Ti(He) sample, and the $F_{Cu/D}$ values are even greater than the products of their corresponding F_{Cu} and F_D. These extremely high $F_{Cu/D}$ values on Cu/Ti(H_2) probably resulted from the synergy of the following three factors: (1) the formation of unique Cu^+/Cu^0 couples where Cu^+ traps electron and Cu^0 traps hole, thus separating electrons and holes on different sites, which is more effective than the sole electron trapping effect by Cu^+ alone; (2) the increased number of V_O and Cu^+/Cu^0 because of annealing in a more reductive atmosphere (i.e., H_2) than He; and (3) the n-doping effect of H atoms into the TiO_2 lattice (i.e., interstitial H) [38].

Another distinct finding from Table 2 and Fig. 9 is the significant enhancement in CH_4 production on the Cu/Ti(H_2) samples. This can be attributed to two possible reasons. First, the abundant Cu^0 species on Cu/Ti(H_2) could facilitate the capture of photo-generated holes, and thus H_2O dissociation favorably occurred at the metallic Cu^0–V_O interface, supplying enough protons (H^+) for the formation of CH_4. Second, the interstitial H species may donate H atoms to promote CH_4 production. This is supported by an additional set of experiments for CO_2 photoreduction on 1%Cu/Ti samples carried out under the following conditions: (1) without H_2O, and (2) with H_2O in the gas stream. Without H_2O, CH_4 production was 0.02, 0.19 and 1.05 μmol g^{-1} on 1%Cu/Ti(UP), 1%Cu/Ti(He), and 1%Cu/Ti(H_2), respectively. The relatively high CH_4 production on 1%Cu/Ti(H_2) suggests the contribution of interstitial H species since the effect of H_2O vapor and adsorbed H_2 can be ruled out. Another important finding was that in the presence of H_2O vapor, the CH_4 production was much more prominent, reaching 0.17, 0.5 and 4.3 μmol g^{-1} on 1%Cu/Ti(UP), 1%Cu/Ti(He), and 1%Cu/Ti(H_2), respectively. For 1%Cu/Ti(H_2), CH_4 production in the presence of H_2O vapor was four times as high as that without H_2O vapor. This clearly indicates that H_2O vapor is the primary donor of H to form CH_4, although interstitial H also contributes to certain extent.

3.5. *In situ DRIFTS for CO_2 photoreduction*

To verify the favorable activation and dissociation of CO_2 on the defective Cu/Ti, in situ DRIFTS for CO_2 photoreduction was conducted on unpretreated and pretreated 1%Cu/Ti. As shown in Fig. 10, exposure of the three 1%Cu/Ti to CO_2 and photo-irradiation induced the formation of bidentate carbonate (b-CO_3^{2-}, at 1578, 1344 cm^{-1}), bicarbonate (HCO_3^-, at 1411, 1220 cm^{-1}), CO_2^- (at 1245, 1672 cm^{-1}) and Cu^+—CO (at 2115 cm^{-1}) [46,47,52]. The formation of CO_2^- suggests that CO_2 can be activated in a way that excess charge, being trapped in defects sites, migrates to adsorbed CO_2 (e.g., $CO_2 + e \rightarrow CO_2^-$) [25,27,53]. The appearance of Cu^+—CO suggests that CO_2 can be dissociated into CO possibly via the CO_2^- intermediate. However, the IR features for the CO_2^- and Cu^+—CO species were very weak on 1%Cu/Ti(UP), but much stronger on 1%Cu/Ti(He) and 1%Cu/Ti(H_2). This difference indicated that compared to the defect-free Cu/TiO_2, the defects on the treated Cu/TiO_2 could act as active sites for CO_2 adsorption, and facilitate the activation and dissociation of CO_2 to CO, agreeing with theoretical

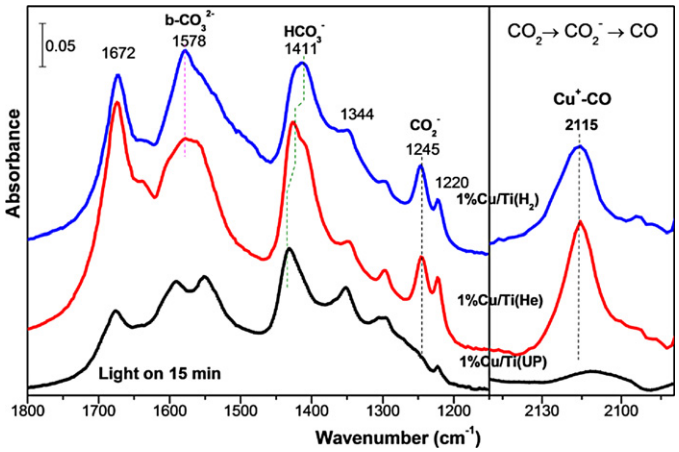

Fig. 10. In situ DRIFTS spectra of CO_2 interaction with the unpretreated and pretreated 1%Cu/TiO_2 under the photoirradiation.

calculation that the reduced TiO_2 with V_O was more favorable for CO_2 binding with accompanying charge transfer to CO_2 [25]. The above in situ DRIFTS result correlates well with UV–vis spectra in Fig. 3, the IR features in Fig. 4 and activity results in Fig. 9, indicating that treated samples have more defect sites for light harvest and CO_2 adsorption, thus having higher activity for CO_2 conversion than unpretreated samples.

To confirm the source of CO_2 reduction products, isotopically labeled $^{13}CO_2$ photoreduction was also performed. The IR spectra of $^{12}CO_2$ and $^{13}CO_2$ interaction on Cu/Ti(He) under photo-irradiation are shown in Fig. 11. Similar IR features in adsorbed species including carbonates and bicarbonates were observed for $^{13}CO_2$ adsorption, except a shift in the spectra compared with the spectrum of $^{12}CO_2$ adsorption. According to the Harmonic equation that is used to calculate the theoretical peak shift for isotopic molecules [47], the vibration frequency (ν) of ^{13}CO (bonded with Cu^+) and $^{13}CO_2^-$ should shift from $\nu(^{12}CO) = 2115\ cm^{-1}$ to $\nu(^{13}CO) = 2068\ cm^{-1}$, and from $\nu(^{12}CO_2^-) = 1245\ cm^{-1}$ to $\nu(^{13}CO_2^-) = 1217\ cm^{-1}$. The 1216 and 2069 cm^{-1} bands in $^{13}CO_2$ adsorption spectrum in Fig. 11 perfectly match the above theoretical calculation, and thus are clearly indication of $^{13}CO_2^-$ and Cu^+—^{13}CO species. This result of labeled $^{13}CO_2$ confirms that the formed CO is indeed derived from the dissociation of CO_2.

The IR results in Figs. 10 and 11 demonstrate the generation of CO_2^-, HCO_3^-, CO and CO_3^{2-} species. In agreement with the

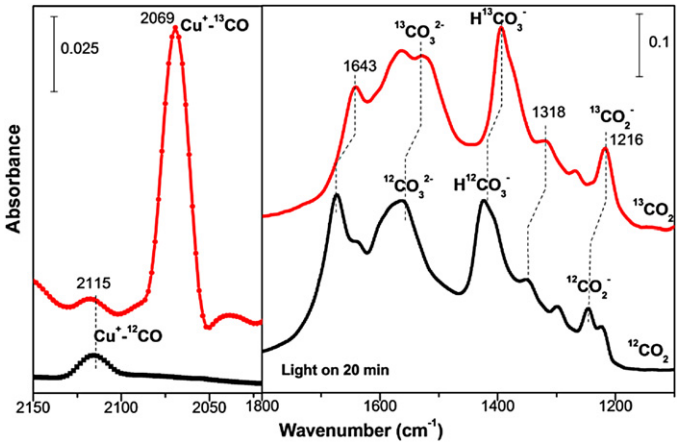

Fig. 11. In situ DRIFTS spectra for $^{12}CO_2$ and $^{13}CO_2$ interaction with 1%Cu/Ti(He) under photoirradiation for 20 min.

mechanism reported in the literature [10,18,47], CO_2^- could be reduced to CO via reaction with H^+ (Reaction 1) or self-transformation (Reaction 2), or direct dissociation by healing the V_O sites (Reaction 3). The formation mechanism of CH_4 may be much more complicated than that of CO, as more electrons and protons are involved in the multi-step conversion. Surface HCO_3^- is a possible intermediate that may be converted to CH_4 (Reaction 4), once dissociated hydrogen is available [10]. Formic acid, methanol, formaldehyde, and CO are also reported as the possible intermediates for CH_4 formation [4,18,54]. However, in the DRIFTS study in this work, even for Cu/Ti(H_2), we have not found direct evidence to explain the CH_4 formation pathway. Future study using both labeled carbon and hydrogen (i.e., $^{13}CO_2$ and D_2O) will be helpful to explore the intermediates and pathways for CH_4 production.

$$CO_2^- + H^+ + e^- \rightarrow CO + OH^- \quad (R1)$$

$$CO_2^- + CO_2^- \rightarrow CO + CO_3^{2-} \quad (R2)$$

$$CO_2^- + [Ti^{3+}{-}V_O{-}Ti^{4+}] \rightarrow CO + [Ti^{4+}{-}O_2^-{-}Ti^{4+}] \quad (R3)$$

$$HCO_3^-, CO, CH_3OH, HCOOH \xrightarrow{e^-} C_{(ads)}{}^{\bullet} \xrightarrow{H^{\bullet}} CH_3{}^{\bullet} \xrightarrow{H^{\bullet}} CH_4 \quad (R4)$$

4. Conclusion

This work comparatively studied the photoreduction of CO_2 with H_2O vapor on Cu/TiO_2 nanoparticles that were engineered with different Cu species and defect sites by low-temperature annealing in different reducing environments. The unpretreated, He-pretreated, and H_2-pretreated Cu/TiO_2 surfaces were dominated by Cu^{2+}, Cu^+, and Cu^+/Cu^0, respectively, and they had increasing activities in CO_2 photoreduction with H_2O vapor. The correlation of photo-activity with material property suggests that the high activity of He or H_2-pretreated Cu/TiO_2 is probably attributed to the synergy of the Cu species and the surface defect sites like oxygen vacancies, which facilitate the separation of electron–hole pairs and promote electron transfer to adsorbed CO_2. The mixture of Cu^+/Cu^0 induced by H_2-reduction seemed to be more active in charge separation than Cu^+ species alone induced by He-pretreatment. The significantly promoted CH_4 selectivity on H_2-reduced Cu/TiO_2 samples is possibly related to interstitial H atoms as well. The in situ DRIFTS study in this work has also revealed a feasible way to study the reaction intermediates and pathways that are important in understanding the mechanism of CO_2 photoreduction.

Acknowledgement

The authors acknowledge the support from American Chemical Society–Petroleum Research Fund (ACS–PRF, Grant #50631-DNI10).

References

[1] S.C. Roy, O.K. Varghese, M. Paulose, C.A. Grimes, ACS Nano 4 (2010) 1259–1278.
[2] K. Mori, H. Yamashita, M. Anpo, RSC Advances 2 (2012) 3165–3172.
[3] M. Anpo, H. Yamashita, Y. Ichihashi, S. Ehara, Journal of Electroanalytical Chemistry 396 (1995) 21–26.
[4] K. Koci, L. Obalova, L. Matejova, D. Placha, Z. Lacny, J. Jirkovsky, O. Solcova, Applied Catalysis B: Environmental 89 (2009) 494–502.
[5] B. Ohtani, Journal of Photochemistry and Photobiology C: Photochemistry Review 11 (2010) 157–178.
[6] J. Rasko, F. Solymosi, Journal of Physical Chemistry 98 (1994) 7147–7152.
[7] O.K. Varghese, M. Paulose, T.J. LaTempa, C.A. Grimes, Nano Letters 9 (2009) 731–737.
[8] C.Y. Zhao, A. Krall, H.L. Zhao, Q.Y. Zhang, Y. Li, International Journal of Hydrogen Energy 37 (2012) 9967–9976.
[9] K. Hirano, K. Inoue, T. Yatsu, Journal of Photochemistry and Photobiology A: Chemistry 64 (1992) 255–258.
[10] D. Uner, M.M. Oymak, Catalysis Today 181 (2012) 82–88.
[11] I.H. Tseng, J.C.S. Wu, Catalysis Today 97 (2004) 113–119.
[12] I.H. Tseng, J.C.S. Wu, H.Y. Chou, Journal of Catalysis 221 (2004) 432–440.
[13] Slamet, H.W. Nasution, E. Purnama, S. Kosela, J. Gunlazuardi, Catalysis Communications 6 (2005) 313–319.
[14] S.Y. Qin, F. Xin, Y.D. Liu, X.H. Yin, W. Ma, Journal of Colloid and Interface Science 356 (2011) 257–261.
[15] Y. Li, W.N. Wang, Z.L. Zhan, M.H. Woo, C.Y. Wu, P. Biswas, Applied Catalysis B: Environmental 100 (2010) 386–392.
[16] W.N. Wang, J. Park, P. Biswas, Catalysis Science & Technology 1 (2011) 593–600.
[17] Q.Y. Zhang, T.T. Gao, Jean M. Andino, Y. Li, Applied Catalysis B: Environmental 123–124 (2012) 257–264.
[18] L.J. Liu, H.L. Zhao, J.M. Andino, Y. Li, ACS Catalysis 2 (2012) 1817–1828.
[19] P.A. DeSario, L. Chen, M.E. Graham, K.A. Gray, Journal of Vacuum Science and Technology A 29 (2011) 0315081–0315087.
[20] J.J. Li, J.L. Zeng, L.S. Jia, W.P. Fang, International Journal of Hydrogen Energy 35 (2010) 12733–12740.
[21] L.J. Liu, C.Y. Zhao, Y. Li, Journal of Physical Chemistry C 116 (2012) 7904–7912.
[22] X.B. Chen, L. Liu, P.Y. Yu, S.S. Mao, Science 331 (2011) 746–750.
[23] A. Danon, K. Bhattacharyya, B.K. Vijayan, J.L. Lu, D.J. Sauter, K.A. Gray, P.C. Stair, E. Weitz, ACS Catalysis 2 (2012) 45–49.
[24] L.B. Xiong, J.L. Li, B. Yang, Y. Yu, Journal of Nanomaterials 2012 (2012) 1–13.
[25] H.Y. He, P. Zapol, L.A. Curtiss, Journal of Physical Chemistry C 114 (2010) 21474–21481.
[26] U. Aschauer, Y.B. He, H.Z. Cheng, S.C. Li, U. Diebold, A. Selloni, Journal of Physical Chemistry C 114 (2010) 1278–1284.
[27] W. Pipornpong, R. Wanbayor, V. Ruangpornvisuti, Applied Surface Science 257 (2011) 10322–10328.
[28] A.T. Brant, S. Yang, N.C. Giles, M.Z. Iqbal, A. Manivannan, L.E. Halliburton, Journal of Applied Physics 109 (2011) 0737111–0737117.
[29] J. Trawczynski, P. Gheeka, J. Okalb, M. Zawadzkib, M.J. Ilan Gomez, Applied Catalysis A: General 409–410 (2011) 39–47.
[30] X.Q. Qiu, M. Miyauchi, K. Sunada, M. Minoshima, M. Liu, Y. Lu, D. Li, Y. Shimodaira, Y. Hosogi, Y. Kuroda, K. Hashimoto, ACS Nano 6 (2012) 1609–1618.
[31] Q.Y. Zhang, E.A. Ackerman, M. Gajdardziska-Josifovska, H.L. Li, Y. Li, Applied Catalysis A: General 400 (2011) 195–202.
[32] C. Deiana, E. Fois, S. Coluccia, G. Martra, Journal of Physical Chemistry C 114 (2010) 21531–21538.
[33] P.A. DeSario, L. Chen, M.E. Graham, K.A. Gray, Journal of Vacuum Science and Technology A 29 (2011).
[34] G. Martra, Applied Catalysis A: General 200 (2000) 275–285.
[35] S.H. Szczepankiewicz, A.J. Colussi, M.R. Hoffmann, Journal of Physical Chemistry B 104 (2000) 9842–9850.
[36] P.M. Kumar, S. Badrinarayanan, M. Sastry, Thin Solid Films 358 (2000) 122–130.
[37] S. Hoang, S.P. Berglund, N.T. Hahn, A.J. Bard, C.B. Mullins, Journal of the American Chemical Society 134 (2012) 3659–3662.
[38] D.A. Panayotov, S.P. Burrows, J.R. Morris, Journal of Physical Chemistry C 116 (2012) 4535–4544.
[39] L. Huang, F. Peng, F.S. Ohuchi, Surface Science 603 (2009) 2825–2834.
[40] G.H. Li, N.M. Dimitrijevic, L. Chen, T. Rajh, K.A. Gray, Journal of Physical Chemistry C 112 (2008) 19040–19044.
[41] V. Gombac, L. Sordelli, T. Montini, J.J. Delgado, A. Adamski, G. Adami, M. Cargnello, S. Bernal, P. Fornasiero, Journal of Physical Chemistry A 114 (2010) 3916–3925.
[42] J.P. Espinos, J. Morales, A. Barranco, A. Caballero, J.P. Holgado, A.R. Gonzalez-Elipe, Journal of Physical Chemistry B 106 (2002) 6921–6929.
[43] W.F. Schneider, K.C. Hass, R. Ramprasad, J.B. Adams, Journal of Physical Chemistry 100 (1996) 6032–6046.
[44] T. Venkov, K. Hadjiivanov, Catalysis Communications 4 (2003) 209–213.
[45] F. Coloma, B. Bachiller-Baeza, C.H. Rochester, J.A. Anderson, Physical Chemistry Chemical Physics 3 (2001) 4817–4825.
[46] W.G. Su, J. Zhang, Z.C. Feng, T. Chen, P.L. Ying, C. Li, Journal of Physical Chemistry C 112 (2008) 7710–7716.
[47] C.C. Yang, Y.H. Yu, B. van der Linden, J.C.S. Wu, G. Mul, Journal of the American Chemical Society 132 (2010) 8398–8406.
[48] I.H. Tseng, W.C. Chang, J.C.S. Wu, Applied Catalysis B: Environmental 37 (2002) 37–48.
[49] W.N. Wang, W.J. An, B. Ramalingam, S. Mukherjee, D.M. Niedzwiedzki, S. Gangopadhyay, P. Biswas, Journal of the American Chemical Society 134 (2012) 11276–11281.
[50] B. Srinivas, B. Shubhamangala, K. Lalitha, P.A.K. Reddy, V.D. Kumari, M. Subrahmanyam, B.R. De, Photochemistry and Photobiology 87 (2011) 995–1001.
[51] N. Sasirekha, S.J.S. Basha, K. Shanthi, Applied Catalysis B: Environmental 62 (2006) 169–180.
[52] J. Baltrusaitis, J. Schuttlefield, E. Zeitler, V.H. Grassian, Chemical Engineering Journal 170 (2011) 471–481.
[53] J. Lee, D.C. Sorescu, X.Y. Deng, Journal of the American Chemical Society 133 (2011) 10066–10069.
[54] C.C. Yang, J. Vernimmen, V. Meynen, P. Cool, G. Mul, Journal of Catalysis 284 (2011) 1–8.